JOURNAL OF APPLIED PHYSICS **118**, 154310 (2015)

Hybrid dispersive media with controllable wave propagation: A new take on smart materials

Andrea E. Bergamini,[1,a)] Manuel Zündel,[2] Edgar A. Flores Parra,[3] Tommaso Delpero,[4] Massimo Ruzzene,[5] and Paolo Ermanni[3]
[1]*Empa, Materials Science and Technology, Laboratory for Mechanical Integrity of Energy Systems, Überlandstrasse 129, CH-8600, Dübendorf, Switzerland*
[2]*ETH Zürich, Institute of Mechanical Systems, Leonhardstrasse 21, CH-8092 Zürich, Switzerland*
[3]*ETH Zürich, Composite Materials and Adaptive Structures Laboratory, Leonhardstrasse 21, CH-8092 Zürich, Switzerland*
[4]*Empa, Materials Science and Technology, Laboratory for Mechanical Integrity of Energy Systems, Überlandstrasse 129, CH-8600 Dübendorf, Switzerland*
[5]*Georgia Institute of Technology, G.W. Woodruff School of Mechanical Engineering, 801 Ferst Drive, Atlanta, Georgia 30332-0405, USA*

(Received 18 May 2015; accepted 8 October 2015; published online 20 October 2015)

In this paper, we report on the wave transmission characteristics of a hybrid one dimensional (1D) medium. The hybrid characteristic is the result of the coupling between a 1D mechanical waveguide in the form of an elastic beam, supporting the propagation of transverse waves and a discrete electrical transmission line, consisting of a series of inductors connected to ground through capacitors. The capacitors correspond to a periodic array of piezoelectric patches that are bonded to the beam and that couple the two waveguides. The coupling leads to a hybrid medium that is characterized by a coincidence condition for the frequency/wavenumber value corresponding to the intersection of the branches of the two waveguides. In the frequency range centered at coincidence, the hybrid medium features strong attenuation of wave motion as a result of the energy transfer towards the electrical transmission line. This energy transfer, and the ensuing attenuation of wave motion, is alike the one obtained through internal resonating units of the kind commonly used in metamaterials. However, the distinct shape of the dispersion curves suggests how this energy transfer is not the result of a resonance and is therefore fundamentally different. This paper presents the numerical investigation of the wave propagation in the considered media, it illustrates experimental evidence of wave transmission characteristics and compares the performance of the considered configuration with that of internal resonating metamaterials. In addition, the ability to conveniently tune the dispersion properties of the electrical transmission line is exploited to adapt the periodicity of the domain and to investigate diatomic periodic configurations that are characterized by a richer dispersion spectrum and broader bandwidth of wave attenuation at coincidence. The medium consisting of mechanical, piezoelectric, and analog electronic elements can be easily interfaced to digital devices to offer a novel approach to smart materials. © *2015 AIP Publishing LLC*. [http://dx.doi.org/10.1063/1.4934202]

I. INTRODUCTION

Control of elastic waves with arrays of periodic piezoelectric shunts for attenuating mechanical vibrations has attracted increased interest. Most of the work has focused on arrays with locally shunted piezoelectric elements aimed at attenuating vibrations in structures.[1–3] This paper reports on an extension of the functionality of the unit cell of periodic structures with piezoelectric elements. Here, the connectivity of the unit cells is defined by the propagation of both mechanical and electrical waves. As we will show in this article, this extension has a remarkable effect on the overall dispersive properties of the resulting medium.

Two approaches for introducing forbidden frequency ranges in the dispersion curves of solid media are extensively reported in literature: phononic crystals (PC) and acoustic metamaterials (AMM). In PCs, bandgaps result from[4,5] periodic modulations of the mass density and/or elastic constants of the material resulting from the basis of the crystal (e.g., diatomic materials[4,6]). Such band gaps exist for wavelengths on the order of the unit cell size and can be complete,[7] i.e., for any direction of propagation, or partial, i.e., direction specific.[8] In metamaterials, on the other hand, the inclusion of suitably designed locally resonating units allows for sub-wavelength modification of the dispersive properties of a medium, as reported by Liu in the mechanical domain.[9] Waves at frequencies corresponding to wavelengths substantially larger than the unit cell size can be attenuated by local resonators. However, metamaterials comprising arrays of identical linear resonators typically address narrow frequency ranges.[10,17]

Other interactions between modes can affect the propagation of waves and induce attenuation. As discussed by Mace and Manconi,[12] mode veering and locking occur, due to weak coupling between two modes, in the vicinity of the crossing frequency of the uncoupled modes, leading to an exchange of energy between them. The manifestation of one phenomenon or the other depends on the product of the group velocities of the interacting modes. A negative product

a)andrea.bergamini@empa.ch

yields locking, while a positive product yields veering. In veering, two modes may approach each other, but instead of crossing, they veer away and diverge. In locking two modes with opposing slope, they interact by creating a pair of attenuating waves[12] with a reduced absolute group velocity. In both cases, reduced transmittance can be observed in the corresponding frequency range.

Both, PCs and mechanical metamaterials, as reported in surveyed literature, consist of a mechanical medium, through which waves propagate and interact with "inclusions" that either scatter them to generate destructive interference at certain wavenumbers or that absorb and dissipate energy through local resonances.[11] The selection and modification of the elastic components defining the properties of media made of artificial atoms provide additional degrees of freedom in the design of these systems. In many of the reported materials, the nature of the inclusions is purely mechanical,[7,9,14] while in some cases, adaptive materials are exploited to modify the geometry of the unit cell,[15] to tune the properties of the locally resonating units,[16–18] or to modify the connectivity of a PC.[19] In the latter cases, what could be defined as the electric moiety of the unit cell is self-contained and only exchanges energy with the mechanical moiety within the unit cell, thus it can be regarded as an inclusion in the mechanical medium. The mechanical component of the unit cell is the only pathway for the exchange of energy with neighboring cells.

Additionally, electrical media are intensively investigated objects in physics as well as in communication science, with the lumped (or discrete) transmission line brought as a classical example for the investigation of electromagnetic wave propagation in media made of artificial atoms. The effect of electrical interconnection of the piezoelectric elements on the dynamic behavior of a structure is explored by dell'Isola[20–22] to control structural vibrations. There, multi-modal damping is pursued by introducing multiple electrical degrees of freedom obtained by interconnecting the electrical resonators, and determining the optimal tuning to address the eigenfrequencies of a finite structure.

This work considers macroscopic media made of "artificial atoms,"[13] that comprise multi-material assemblies. Such assemblies have the potential to include power-transducing materials or even analog circuits. The novelty of this contribution lies in the extension of the functionality of the atoms with respect to media with piezoelectric inclusions previously presented, by the addition of connectivity in the electrical domain. This enables the simultaneous propagation of energy in the mechanical and electrical domains. In this contribution, we will discuss the effect of the interaction between wave modes in the electrical and mechanical domains on the propagation of mechanical waves in the proposed hybrid medium.

II. HYBRID MEDIA

The medium investigated in this work is characterized by periodicity in both the electrical and mechanical domains. The mechanical component consists of an aluminum beam (Fig. 1(a)) onto which piezoelectric elements are mounted.

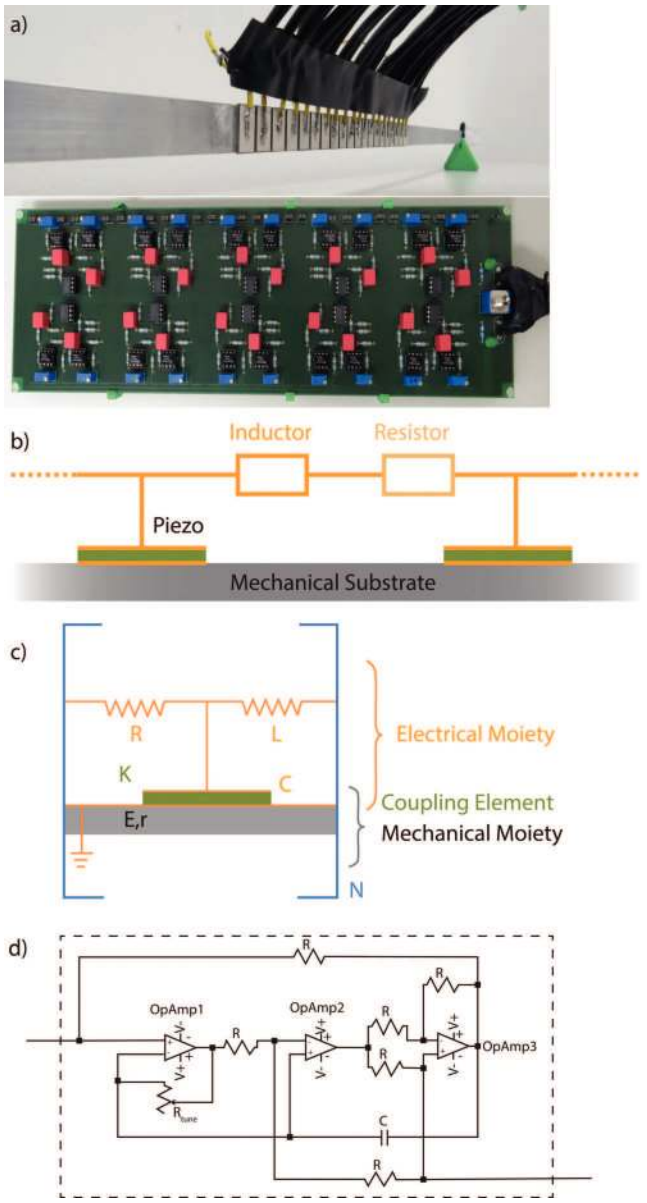

FIG. 1. Hybrid electromechanical phononic crystal (hPC): A finite size sample of the proposed hybrid dispersive medium. Mechanical waves propagate through the aluminum substrate on which piezoelectric elements are applied (top of panel (a)). The electrical medium consists of the piezoelectric elements connected with inductive elements as shown in (b). The latter are realized using an active circuit (bottom of panel (a)) that allows for easy tuning of the inductance value, rather than with physical inductors. Panel (c) shows the schematic of the unit cell, consisting of a mechanical, an electrical moiety coupled by the piezoelectric element. Finally, panel (d) shows the circuit[23] used to synthesize the inductors.

The electrical component (Fig. 1(a)) is realized by combining inductors with piezoelectric elements serving the dual purpose of capacitors in a lumped transmission line and electromechanical transducers offering an interface between the electrical and mechanical moieties of the medium. The resulting electrical medium is defined as a lumped transmission line. The periodicity of the mechanical moiety is spatial as it is defined by the arrangement of the piezoelectric elements. Conversely, the periodicity of the electrical moiety is defined not only by the inductance values of the lumped transmission line but also by the spatial periodicity of the

piezoelectric elements on the aluminum substrate that form the discrete structure of the electrical network.[24]

The appeal of a hybrid electromechanical dispersive medium lays in the convenient modification of the properties of the electrical moiety of the unit cell and thus of the dispersion modes through the use of electrical components. Given the interaction between the two moieties of the hybrid medium provided by the piezoceramic elements, we expected the electrical medium to affect the propagation of waves in the mechanical medium. As we will show, based on its dispersion properties, the system operates in a sub-wavelength regime, i.e., the unit cell size is substantially smaller than the length of the waves it affects. As such, it is deemed appropriate to regard this system as an equivalent hybrid medium in the metamaterial sense.[25]

Here, the inductive elements of the electrical component are realized using an analog circuit described in Section III. This choice for the realization of part of the electrical moiety allows for accurate control of the value of the inductive elements and implies the integration of a tunable component into the unit cell of the periodic medium. By changing the value of the variable resistor R_{tune} (Fig. 1(d)), the inductance value of the element can be set.

The interconnected electrical components of the medium offer more complex dynamics than the previously proposed unit cells with local resonators, by exploiting the additional degrees of freedom. These added degrees of freedom enable modifying the unit cell symmetry in the electrical domain by introducing features, such as a diatomic lattice, comprising alternating inductances, or more complex patterns. In this work, a monoatomic unit cell of the hybrid medium, same inductance across all cells, is investigated and compared to a monoatomic unit cell of the locally shunted resonator. The same process is then repeated for a diatomic unit cell, alternating inductances, of the hybrid medium.

III. METHODS

In the following, we describe the numerical and experimental methods used for the investigations.

A. Numerical calculation of the dispersion curves of the hybrid medium

We calculated the dispersion curves of the hybrid medium using the finite element method (COMSOL Multiphysics, V4.4) by analyzing the eigenfrequencies of the unit cell modeled considering Floquet-Bloch boundary conditions. A similar implementation, for a purely mechanical system, is presented, for example, in Ref. 7. In the model of the one-dimensional hybrid medium discussed in this work, periodic boundary conditions were imposed on both, the mechanical and the electrical moieties. For the mechanical moiety, the Floquet-Bloch boundary conditions implemented by COMSOL were applied to obtain $u_{r_N} = u_{l_N} e^{-iak}$, where u_{r_N} and u_{l_N} are, respectively, the mechanical degrees of freedom on the right side and left side of the unit cell, k is the wavenumber, and a is the lattice constant of the hybrid phononic crystal (hPC). For the electrical moiety, the periodicity was implemented directly by imposing Eq. (1) using the *Global ODEs and DAEs* physics of COMSOL. Equation (1) is derived by first relating the voltage across the Nth piezoelectric element, V_N, and the voltages across the adjacent piezoelectric elements V_{N-1} and V_{N+1} through the Floquet-Bloch boundary conditions as seen in Eqs. (2) and (3). Next, the relation between voltage and current in the unit cell leads to the ordinary differential equation, Eq. (4). In the latter, L is the value of the inductor in the unit cell, R is the value of the resistor, I_{l_N} and I_{r_N} are the currents flowing in and out of the unit cell (from left to right, see Fig. 2. Lastly, the currents I_N resultant from the charges q_N on the top electrodes of the piezoelectric elements are related through the first time derivative $I_N = I_{l_N} - I_{r_N} = \dot{q}_N$. Time, t, is taken into account assuming harmonic oscillating charges ($q_N = Q_N \sin(\omega t)$)

$$L\ddot{q}_N + R\dot{q}_N = V_N(e^{-iak} + e^{iak} - 2), \tag{1}$$

$$V_{N-1} = V_N e^{iak}, \tag{2}$$

$$V_{N+1} = V_N e^{-iak}, \tag{3}$$

$$L(\dot{I}_{l_N} - \dot{I}_{r_N}) + R(I_{l_N} - I_{r_N}) = V_N(e^{-iak} + e^{iak} - 2). \tag{4}$$

The geometry of the unit cell was defined according to the geometry of the experimentally investigated sample, see Fig. 3. The lattice constant a for the monoatomic unit cell was 10 mm, the thickness h_s of the aluminum substrate was 1.58 mm, its width (out of plane dimension) b was 12.7 mm. The model is a 2D plane stress approximation. The out-of-plane dimension b was an input parameter to COMSOL used to scale the electrical charges. The piezoelectric element had a thickness h_p of 1 mm, a length l_p of 8.9 mm, and width b of 12.7 mm.

The material properties were the ones of *aluminum* described in the COMSOL materials library ($E_s = 70$ GPa, $\rho_s = 2700$ kg/m^3, $\nu = 0.3$), while the properties of the STEMiNC SM112 implemented were the ones provided by the supplier for the proprietary SM112 material ($C_{11} = 84$ GPa, $k_{31} = 0.34$, $\epsilon_{33}^T/\epsilon_o = 1600$, $\rho_p = 7900$ kg/m^3). For the investigation of the monoatomic unit cell, a resistance $R = 451\,\Omega$ was implemented in the numerical model to account for the measured average resistance in the experimental sample. The selected values for the inductors and resistors, L and R, respectively, were selected to obtain the desired crossing frequency.

For the monoatomic unit cell of the hybrid medium, an inductance $L = 0.37$H, corresponds to a crossing frequency, $\omega_c = 10$ kHz, with the A_0 mode of the mechanical substrate. Similarly, for the monoatomic unit cell of the locally shunted resonator, an inductance $L = 0.16$H, corresponds to a crossing frequency, $\omega_c = 10$ kHz, with the A_0 mode of the mechanical substrate. In the case of the monoatomic cell, both the local and hybrid systems were tuned to ensure mode crossing at 10 kHz thus the difference in inductance values.

In the case of the diatomic cell, the inductance values were kept the same for both the local and hybrid systems. As a result, for the hybrid medium, $L_1 = 1.3$H, $L_2 = 2.6$H, and $R_1 = R_2 = 0\,\Omega$, yielded a crossing frequency of the acoustic electrical mode with the A_0 mode in the vicinity of $\omega_{c1} = 2.1$ kHz, while the optical mode with the A_0 mode crossed around $\omega_{c2} = 5.2$ kHz. For the local resonator case,

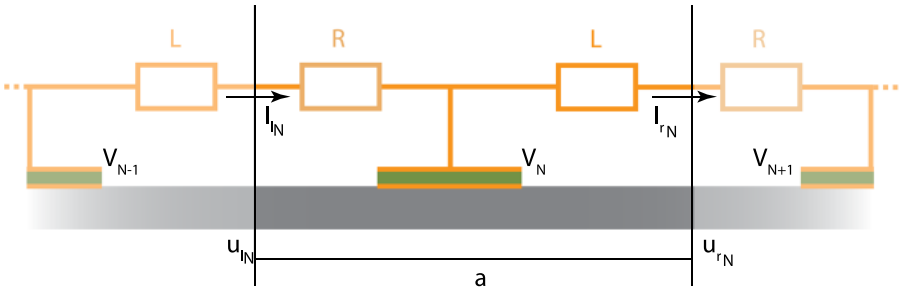

FIG. 2. Variables in the definition of Floquet-Bloch boundary conditions in the electrical domain.

the A_0 mode was intercepted at the two resonant frequencies, $\omega_{c1} = 2.5$ kHz and $\omega_{c1} = 3.5$ kHz, which correspond to the two zero group velocity modes of the locally shunted LC circuits. Each piezoelectric element had a capacitance of about 1.65 nF.

We obtained the dispersion curves by solving the eigenvalue problem of the coupled system for the first three to five eigenmodes while imposing $k = [0 \ldots \frac{\pi}{a}]$ in a parametric sweep. As the imposed k-values are real, no solution was found for spatially attenuated waves that would imply complex wavenumbers, as in the case of mode locking.

B. Numerical calculation of the transmittance of a hybrid phononic crystal

For the calculation of the transmittance of a finite hPC, we modeled the experiment described in Sec. III C using COMSOL Multiphysics V4.4. The dimensions of the modeled beam were 1.58 mm × 12.7 mm × 800 mm ($t \times b \times l$). In the center portion of the structure, a hPC with unit cell size of 10 mm was added, consisting of 20 unit cells positioned between 300 mm and 500 mm from the origin (left end of the structure) as seen in Fig. 3. Each unit cell had a piezoelectric element with the same dimensions as the ones used to calculate the dispersion curves. We defined a perfectly matched layer as the boundary condition at either end of the structure to suppress the reflection of mechanical waves. We modeled the inductive and resistive components using the *electric circuit* physics of COMSOL. The selected values for the inductors and resistors, L and R, respectively, as well as for the geometry of the unit cell and the material properties were the same as for the calculation of the dispersion curves in order to establish a direct correlation between the dispersion curve of the hybrid medium and the transmittance of a finite hPC. The mechanical transmittance of the hPC was calculated by taking the ratio of the spatial average of the velocity amplitudes, over a region with 100 mm length, before and after the periodic arrangement

$$T(\omega) = \frac{v_{a,out}}{v_{a,in}} = \frac{mean(v_a(\omega, x \in [500\,\text{mm}, 600\,\text{mm}], y \in [0, h_s]))}{mean(v_a(\omega, x \in [200\,\text{mm}, 300\,\text{mm}], y \in [0, h_s]))}. \quad (5)$$

As depicted in Fig. 3, the system was excited mechanically by a discrete force $F(t)$ applied 150 mm from the origin. The steady state frequency response of the system was calculated over the frequency range of interest.

C. Experimental measurement of the transmittance and dispersion of a hybrid phononic crystal

The system used for the experimental investigation of the wave propagation through the hPC essentially matched the system we investigated numerically. The mechanical substrate was a 6061 aluminum alloy beam purchased from McMaster Carr Supply Company. The piezoelectric elements SM112 PZT purchased from STEMiNC had the same dimensions as the ones used in Secs. III A and III B. However, a slightly greater width, b, of 13.1 mm had to be chosen since the product was unavailable in the specific dimensions used for the numerical analysis. The piezoelectric elements were positioned on the substrate with the help of a custom made mask and fixated to it using conductive two-component epoxy adhesive. The resulting structure is shown in Fig. 1(a).

The inductive elements needed to implement the lumped transmission line were realized using active analog circuits. The term "active" refers to the fact that the response of the system is obtained using three operation amplifiers, which are active electronic components. Four reasons prompted us to opt for synthetic inductors rather than physical inductors made of wound conductors: (a) the physical components for

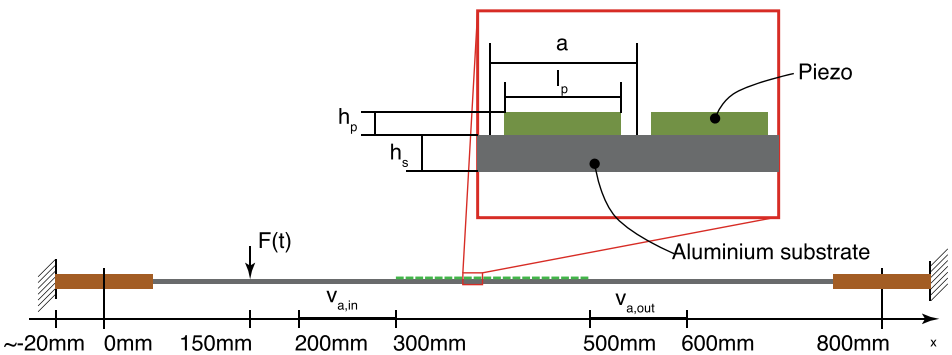

FIG. 3. Overview and dimensions of the investigated hPC with detailed view of two unit cells. The dimensions a, l_p, h_s, h_p are detailed in the text.

the realization of the needed inductivities are quite large and heavy, (b) the tolerances of high quality inductors with large inductance values are of the order of 5% to 10% of the nominal inductance value which was deemed not satisfactory for this proof of concept. Further investigations on the robustness of the system against variation of the L-value will be carried out at a later stage. (c) Synthetic inductors are not physically coupled to RF signals from the environment as conventional inductors are and thus less prone to parasitic effects. (d) The analog circuits can be easily interfaced to digital devices by replacing the analog tunable resistor R_{tune} with a digital potentiometer. This allows for the inclusion digital devices—possibly offering central or distributing computing capabilities—into the unit cell. The synthetic inductors were realized using the circuit described in Ref. 23. As the operational amplifiers components used in the circuit were dual (so two OpAmp per integrated circuit) and 20 synthetic inductors were needed, the array was designed as an array of 10 couples of inductors. The layout of one double unit is shown in Fig. 4. Each inductor comprised three OpAmps. One dual (OpAmp1A/B, in the figure) is completely part of one unit, while OpAmp2 is shared. The resistivity value of the fixed resistor was 10 kΩ, the capacitance of the capacitor was 10nF. The nominal resistivity of the potentiometer R_{tune} was 50 kΩ. For OpAmp1, we used type TL082CN, whereas for OpAmp2, we used type LM6172. The array of inductors was powered by a laboratory power supply delivering two channels with ±7 … 15 V relative to ground. The average capacitance of the piezoelectric elements was $\langle C_p \rangle$ 1.59 pF ± 0.05 pF. Accordingly, in order to achieve characteristic frequency of the order of 10 kHz, inductivity values of the order of $L \approx 0.16$ H are needed. The average resistivity of the 20 inductive elements tuned for a coincidence frequency of 10 kHz was $\langle R \rangle = 451\ \Omega \pm 86\ \Omega$.

The synthetic inductors and the piezoelectric are connected using shielded cables to reduce RF interference. The tested hPCs had a maximum of 20 active unit cells (shown in Fig. 1(a)). Prior to performing transmittance measurements, we tuned the inductors in each cell of the transmission line to match the same frequency, thus also compensating for minor deviations in the capacitance of the piezoelectric elements (of the order of 3%). The tuning was performed by maximizing the voltage response across the piezoelectric element, as the whole RLC resonator (i.e., the piezoelectric element and the synthetic inductor in series) was excited with an AC voltage signal at the desired frequency, while the unit cell was disconnected from the others.

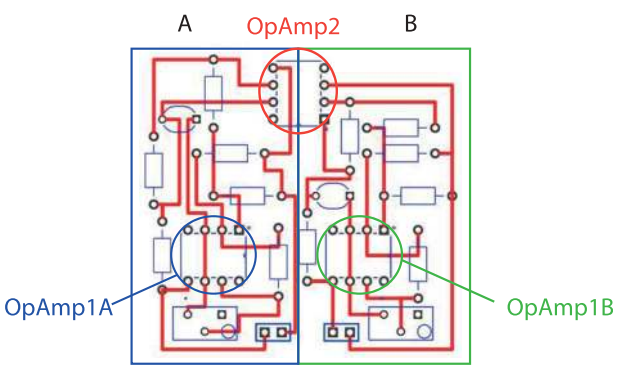

FIG. 4. Layout of a double inductor unit.

We excited the structure using an additional piezoelectric element attached approximately 150 mm from the origin, i.e., in the same position where the discrete force was applied in the numerical model. The piezoelectric element was excited using a tone burst centered around 10 kHz with a duration of four cycles. This kind of excitation allowed us to bundle energy in the frequency range of interest while having shorter measurement sequences than we would have needed using a chirp signal. The low voltage tone burst signal was generated by an Agilent 33220 A arbitrary waveform generator and was amplified to a maximum of 50 V using a Trek PZD350 Dual high voltage power amplifier.

The out of plane velocity on the surface of sample was measured using a Polytec PSV 400 scanning laser vibrometer. The transmission properties of the hPC were calculated based on velocity amplitude averaged over regions extending 100 mm on either side of the hPC with a spatial resolution of approximately 2 mm. The velocity signal was acquired with 128 kHz sampling frequency. For each point, we measured the response of the system to 25 consecutive tone burst signals to obtain reliable data. In Fig. 5, we report the velocity spectra in the specimen as a function of the position. We carried out a Fast Fourier transform of the time-domain data for the out of plane velocity along the length of the sample to obtain the frequency response. The numerical investigation was carried out conceptually in the same way, except for the fact that the behavior of the system was investigated in a frequency response analysis, thus the data were directly available from the solution.

In Fig. 5, we can see that in the portion of the sample occupied by the hPC, the velocity amplitudes are substantially lower than in the portions left (upstream) and right (downstream) of the hPC. This difference is due to the larger mass and stiffness of the hPC compared to the neat substrate. Accordingly, the recorded velocity amplitude is smaller for obvious energy conservation reasons. As the wave packet traverses the hPC, the change in wave velocity amplitude as a function of frequency becomes visible, whereas in the 10 kHz region, where most of the energy is concentrated (as shown by the high amplitudes upstream of the hPC), the amplitude is strongly reduced, leading to the very low velocity amplitudes recorded downstream of the hPC for the coincidence frequency of the electrical and mechanical modes, i.e., around 10 kHz. Further processing of these data can be carried out to obtain an approximation of the mechanical component of dispersion curves of the hPC. These dispersion curves can be obtained as described in Ref. 29 and are shown in Fig. 6. These plots display the region of interest around the coincidence frequency of 10 kHz. While the absolute value of the time-FFT is considered in the plots, complex spectrum resulting from the space-FFT is considered. The "waviness" in the real part of the dispersion curve, similar to the S-shape observed in local resonators, points to interactions between the mechanical and electrical modes. The imaginary part of the dispersion curve is related to the spatial wave attenuation.

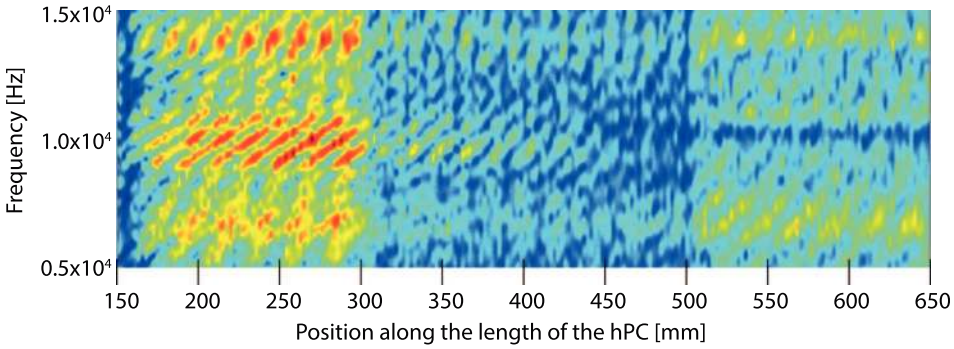

FIG. 5. Wave velocity amplitude as a function of frequency and location along the sample, where the hPC with 20 interconnected cells occupies the region between 300 mm and 500 mm, from the origin, as defined in Fig. 3. The amplitude, in arbitrary units is displayed by the color in the plot.

IV. RESULTS AND DISCUSSION

A. Monoatomic unit cell

We shall now direct our attention to the behavior of a finite sample of the proposed hybrid medium, as observed in experiments and multi-field numerical models. Then we will elucidate it based on the dispersion curves of the infinite medium. We will compare the response of the hybrid medium to the one of the mechanical medium with locally resonant piezoelectric inclusions,[16,17] where the main difference is that the piezoelectric elements are shunted to ground instead to the neighboring piezoelectric elements.

We investigated, experimentally and numerically, the transmission of mechanical waves through a finite sample of the material consisting of 20 unit cells. The transfer function for the structure was calculated from numerical and experimental results, following the procedure described in Section III. As previously mentioned, the synthetic inductors of both systems (i.e., the hybrid medium and the array of local resonators) were tuned so that the frequency at which the electrical and the mechanical modes interacted, i.e., the coincidence frequency, was centered around 10 kHz.

The dispersion properties of the metamaterial were calculated numerically based on a unit cell of the very same hybrid medium onto which Floquet-Bloch boundary conditions were imposed. The $k-\omega$ dispersion curves were calculated by imposing $k = [0 \ldots \frac{\pi}{a}]$, where a denotes the spatial periodicity of the system (i.e., the unit cell length) to cover the first irreducible Brillouin Zone (BZ). The dispersion properties of the system with locally resonant cells as well as the interconnected medium were calculated, assuming the same geometric and electrical parameters, except for the connectivity of the electrical medium.

The dispersion curves of the system with locally resonant cells and the hybrid medium can be compared to the dispersion curves of the uncoupled mechanical system, which is equivalent for both the dispersion of an LC circuit and a lumped LC transmission line, respectively. As seen in Fig. 7(a), an excellent correlation exists between the dispersion curves of the hybrid medium and the uncoupled modes of the purely mechanical (open circuit over the piezoelectric elements) and purely electrical (a lumped transmission line with the same electrical parameters as in the hybrid medium) media (Fig. 7(a)), calculated numerically and analytically. The blue and red lines in Figs. 7(a) and 7(b) represent the first and second modes of the media, respectively, and the purple dashed and green dotted lines represent the dispersion curves of the uncoupled electrical and mechanical modes, respectively. The accuracy of the developed models could be verified experimentally by comparing the predicted (dashed red line in Figs. 7(c) and 7(d) and experimentally measured (solid blue line) transmittance of the finite PCs.

Fig. 8 gives insight into the nature of the modes of these dispersion diagrams. The displacement and electric field mode shapes in the transverse direction were obtained from the eigenfrequency analysis used to calculate the dispersion curves. Mode shapes (IIa) and (IVa) are predominantly mechanical in nature. Accordingly, the—inhomogeneous—field distribution in the piezoelectric element is dominated by the direct piezoelectric coupling by virtue of which mechanical strain induces a polarization of the actuator. Conversely, modes (Ia) and (IIIa) are predominantly electrical as seen

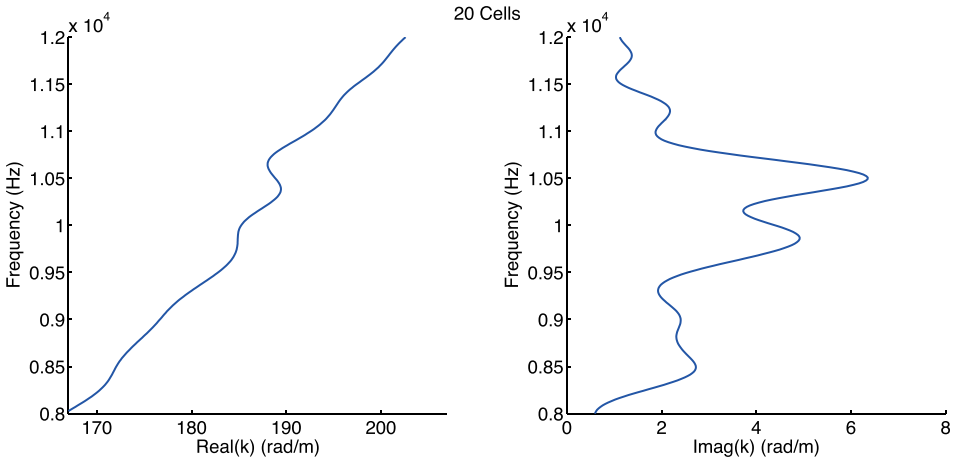

FIG. 6. Approximate $k-\omega$ dispersion data obtained from the 2D FFT of the velocity data recorded in the hPC region of the investigated sample.

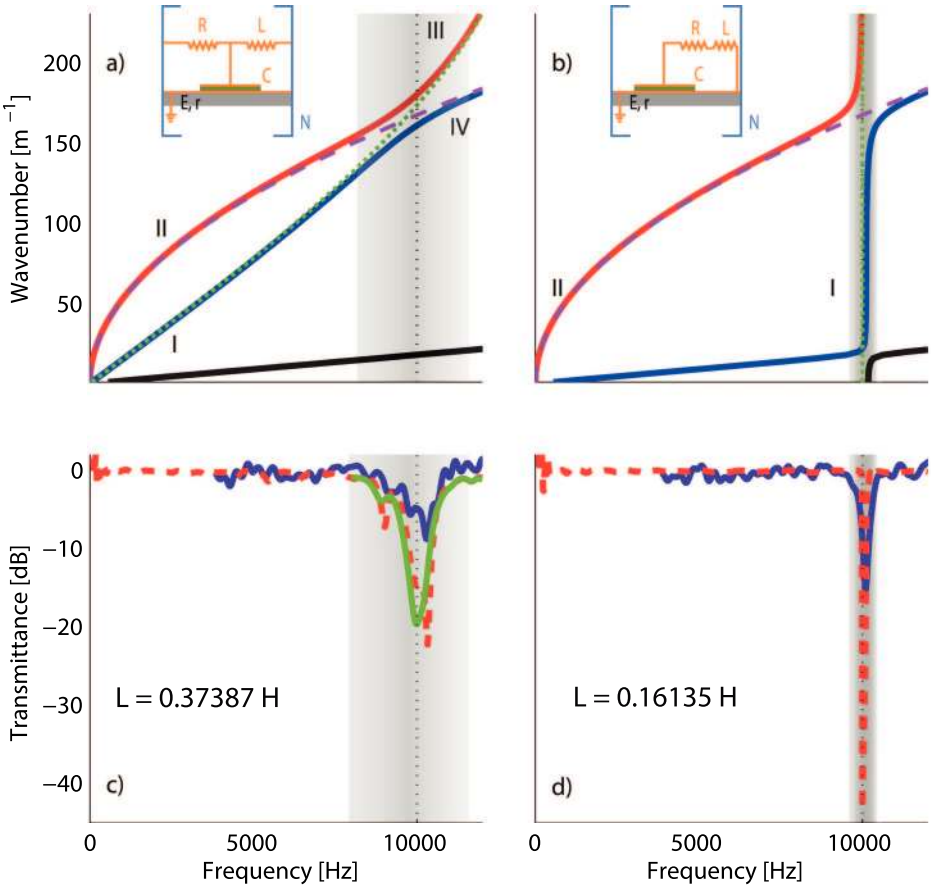

FIG. 7. Transmittance and dispersion curves of the media consisting of monoatomic unit cells. The plots on the left refer to the hybrid dispersive medium, the ones on the right to the arrays of local resonators. The curves in (a) and (b) represent dispersion of the first modes in the media. The curves in (c) and (d) represent the predicted and experimental transmittance of the finite PCs.

from the—homogeneous—electric field distribution across the piezo element. Here, the piezoelectric elements are acting as capacitors in the lumped transmission line. The field in the piezo is dictated by the propagation of electric waves along the electric moiety of the medium. These observations are in line with expectations as the purple dashed curve corresponds to the transverse mechanical mode, while the green dotted curve corresponds to the lumped transmission line and after veering mode switching occurs.[12]

In the medium with locally resonant units, the piezoelectric resonators contribute a k–independent, zero group velocity, mode that crosses several mechanical modes (Fig. 7(b)), including the one related to the asymmetric A_0 Lamb's waves of the plate, as presented, for example, in previous work.[26] As seen for the hybrid medium, the electric field distribution of modes shapes (Ia) and (IIa) in Fig. 8 indicates that they are electrical and mechanical in nature, respectively.

The comparison of the measured and calculated transmittance curves reveals a good match (Figs. 7(c) and 7(d)) between experimental and numerical results (note the dB scale) for both the hybrid medium and for the local resonator system. While the local resonators cause a sharp and pronounced dip in the transmittance of the system, the

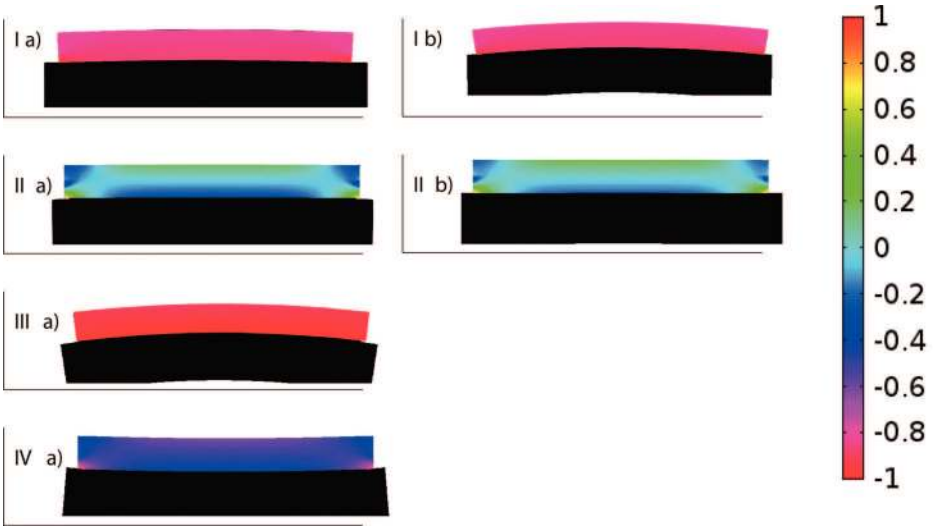

FIG. 8. The mode shapes (out of plane mechanical displacement represented by the shape, and electric field across the thickness of the piezo represented by the color distribution) in the figure refer to the Roman numerals in Figs. 7(a) and 7(b). These mode shapes were normalized by the root mean square and the transverse electric fields were plotted using a symmetric color range from −1 to 1.

interconnected system is characterized by a shallower but broader response. Moreover, there is a good correlation between the frequency range over which the electrical and mechanical modes interact and the range over which strong attenuation of the mechanical waves occurs (Figs. 7(a) and 7(b)). Since energy can propagate along the electrical moiety, boundary conditions can be imposed in the electrical domain to modify the response of the system. The latter is an additional feature that differentiates the hybrid medium from the corresponding array of local electromechanical resonators and underscores the potential of introducing an electrical moiety. In the experimental set-up, damping material was added at the extremities of aluminum beam hosting the finite 20 unit cell PC to increase damping and minimize mechanical wave reflections at the boundaries as seen in Fig. 7(c). In the numerical model, perfectly matched layers were implemented at the ends of the beam to absorb mechanical waves. To achieve this same effect along the electrical domain, reflections were minimized through impedance matching of the lumped transmission line. Assuming the line to be lossless, the characteristic impedance is defined as $Z_o = \sqrt{\frac{L}{C}}$, where L is the inductance value and C is the capacitance of a piezoelectric element. A reflection-free lumped LC transmission line can then be achieved by terminating the line with a resistance $R_o = Z_o$. By eliminating the wave reflections from the electrical line, the transmittance response becomes smoother as the anti-resonance peaks disappear, as shown in Fig. 7(c) by the solid green curve.

B. Diatomic unit cell

To further exploit the wave attenuation capabilities of the hybrid dispersive medium, where the electrical moiety has the potential to be readily modified, we introduce a diatomic cell characterized by alternating inductance values. All material and geometric parameters are kept unchanged with respect to the previously studied monoatomic unit cell, except for the unit cell length which is now $2a$ to account for the doubling of the spatial periodicity. To better appreciate the response of the diatomic cell of the hybrid medium, we will again compare it with the response of the corresponding diatomic local resonant cell. As expected, the system with locally shunted piezoelectric elements and alternating inductance values yields two narrow attenuation peaks in the vicinity of the frequencies corresponding to each inductor, see Fig. 9(b). The diatomic local resonant shunts are characterized by two k-independent, zero group velocity, modes which interact with the mechanical modes of the aluminum substrate. These regions of interaction between the mechanical and electrical modes correspond to the frequency ranges of energy exchange as seen for the array of local resonators with identical inductors.[17]

Conversely, the diatomic cell of the hybrid medium has a more complex response. Fig. 9(c) shows the calculated transmittance for a finite hPC consisting of 10 diatomic unit cells, each comprised two piezoelectric elements and two inductors. In the figure, we notice two regions of increased attenuation. The gray shading in Figs. 9(a) and 9(c) shows the qualitative frequency correspondence between these higher attenuation regions and the regions where veering and/or locking are observed in the dispersion curves. The smaller inductance governs the position of the optical mode, which has a negative group velocity as seen in Fig. 9(a), and thus also controls the location of the locking. As discussed in Ref. 12, this leads to an exchange of energy between the modes that increases as they approach the wavenumber and frequency at which they would cross, if veering did not occur. In the present system, as opposed to the one discussed in Ref. 12, one of the two modes interacting has an electrical

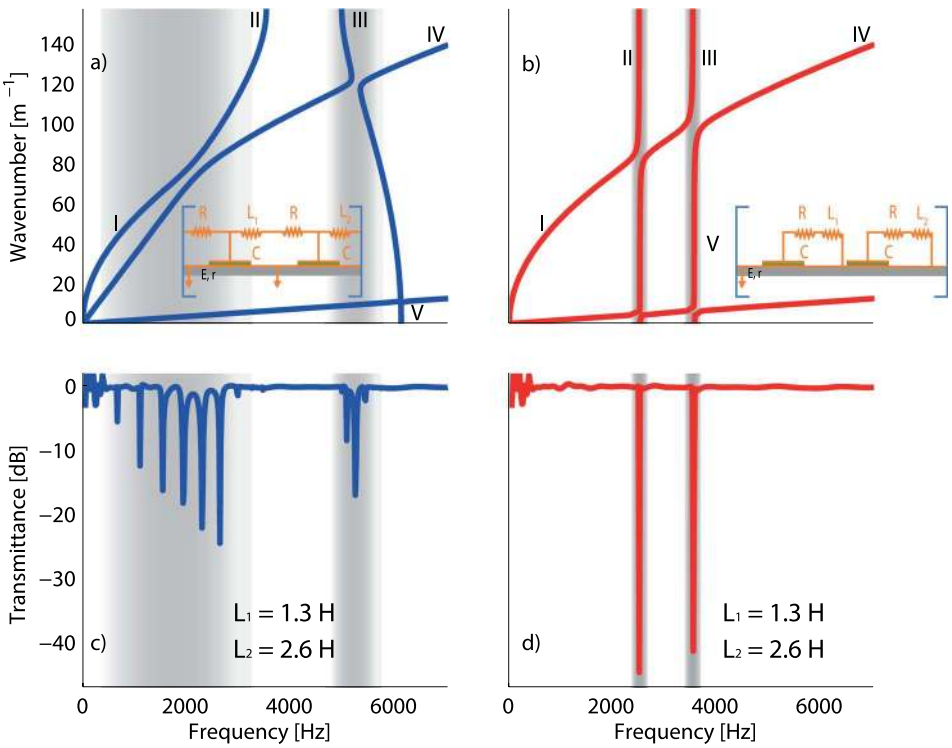

FIG. 9. Transmittance and dispersion curves of the media consisting of diatomic unit cells. The plots on the left refer to the hybrid dispersive medium, the ones on the right to the arrays of local resonators. The curves in (a) and (b) represent dispersion of the first modes in the media. The curves in (c) and (d) represent the predicted transmittance of the finite PCs.

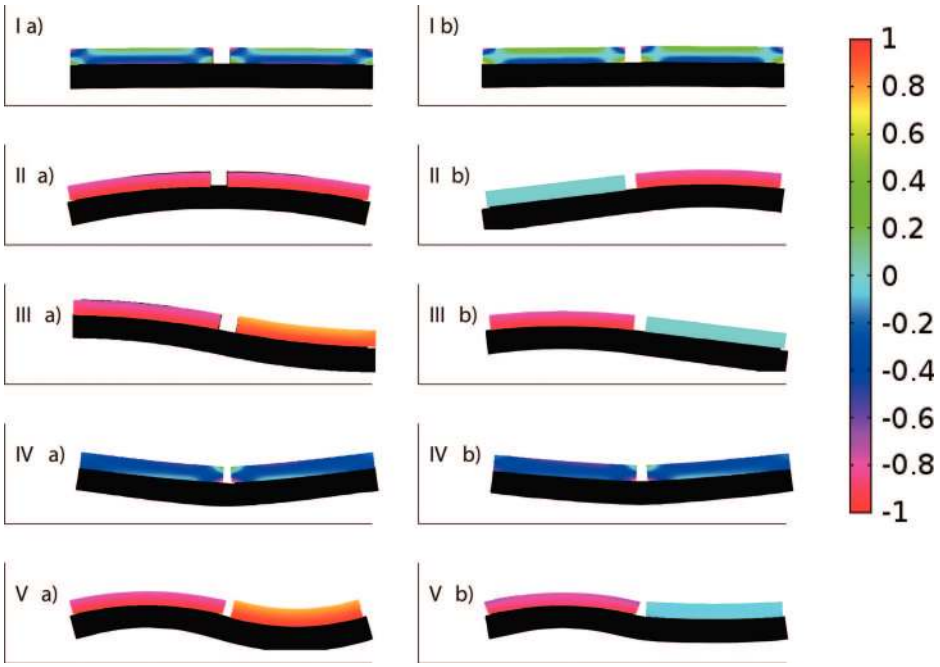

FIG. 10. The mode shapes (out of plane mechanical displacement represented by the shape, and electric field across the thickness of the piezo represented by the color gradient) in the figure refer to the Roman numerals in Figs. 9(a) and 9(b). These mode shapes were normalized by the root mean square and the transverse electric fields were plotted using a symmetric color range from −1 to 1.

character. The exchange of energy between the two modes explains the attenuation of the mechanical waves that propagate through the medium. In the second case (locking), the group velocities of the two modes are opposite in sign. Again, Ref. 12 offers a physical interpretation of the process that leads to the attenuation of the mechanical waves in the system. For locking modes, it is shown that in the frequency region of interest, no real values of the wavenumber describe the system. Waves with a purely imaginary wavenumber are said to be evanescent, i.e., to exponentially decay in amplitude over space.[30]

The transmittance curve in Fig. 9(c) is calculated based on a lossless transmission line, where the resistivity of the line is zero. The large number of attenuation peaks in the latter can be attributed to the small number of unit cells, where degeneration of modes due to the occupation of the same frequency by multiple modes of the finite transmission line leads to multiple peak splitting, with theoretically as many peaks as existing degrees of freedom. At a higher frequency, an additional attenuation peak is visible corresponding to the locking of the electrical optical mode and the mechanical A_0 mode (line connecting I and IV in Fig. 9(a)).

Analogously to a diatomic spring mass system, where the masses of the optical mode oscillate out of phase with equal amplitude for the wavenumbers at the boundaries of the considered wavenumber range,[27,28] $k = [0; \frac{\pi}{a}]$, the electric field mode shapes of the optical mode (Figs. 10(IIIa) and 10(Va)) of the interconnected diatomic inductance cell also exhibit equal amplitude but inverse polarization. Moreover, the unit cell displacements engendered by such fields agree with the imposed periodic boundary conditions. For the long wavelength limit (location V in Fig. 9(a)), the mode shape displacements on the left and right hand side of the unit cell are equivalent (Fig. 10(Va)). Likewise, for the short wavelength limit (location III in Fig. 9(a)), the deformations engendered by the electric fields are such that the displacements on the left and right hand sides of the unit cell have equal amplitude but opposite direction (Fig. 10(IIIa)). Furthermore, the modes corresponding to the mechanical curves can be readily identified by the inhomogeneous distribution of the electric field over the piezo elements (Figs. 10(Ia) and 10(IVa)). Lastly, the acoustic mode (location II in Fig. 9(a)) is characterized by equally polarized uniform electric fields (Fig. 10(IIa)).

In contrast with the hPC, Figs. 9(b) and 9(d) show the transmittance and dispersion plots for the corresponding locally resonating system. Due to the lack of electrical connectivity between the elements of the PC, no degeneration of the attenuation peaks is observed. This results in two neat attenuation peaks corresponding to the interaction of the *k*-independent electrical modes III and the lower frequency parallel mode going through II in Fig. 9(b) with the mechanical A_0 mode (curves I–IV). These attenuation peaks display substantially larger amplitude than those in Fig. 9(c), but over a much narrower frequency range. The modes displayed in Fig. 10(Ib) through 10(Vb) also confirm the different characters of the calculated modes as well as an effect of the diatomic nature of the unit cell on the electrical mode.

V. CONCLUSIONS AND OUTLOOK

In the presented hybrid medium, we have introduced additional electrical modes that interact with the mechanical modes of the medium to exploit veering and locking, as elucidated by using numerical models and analyzing the nature of the modes. Indeed, the frequency range at which strong attenuation of mechanical waves traversing the hybrid medium is observed, coincides with the range of frequencies at which veering or locking of electrical and mechanical modes

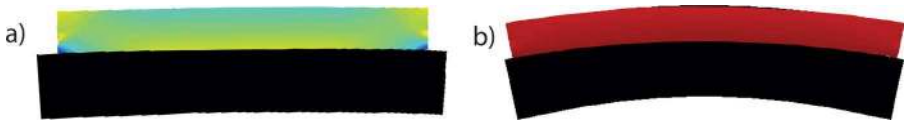

FIG. 11. (a) Non-periodic unit cell subject to bending moments. (b) Non-periodic unit cell with electric potential applied across piezoelectric element.

in the dispersion diagram is observed. The effect of these phenomena on the propagation of mechanical waves in a sub-wavelength regime, which can be of special interest in a number of engineering applications, has been shown numerically and experimentally.

The integration of a mechanical and electrical moiety, consisting of a simple analog circuit, to create a hybrid medium allows for the adaptation of both the mechanical and the electrical expression of its dispersion properties by exploiting the tunability of the electric impedance. The electrical moiety is realized by a simple analog circuit and further offers an ideal interface to digital devices (e.g., by integrating digital potentiometers), such as central or distributed computing units. In the presented medium, we can thus state that an analog circuit is an integral part of a material. In this sense, we claim that the hybrid medium represents a demonstration of the hardware element of a new class of smart materials comprising mechanical, analog, and—potentially—digital electric elements, with tunable and programmable properties.

APPENDIX: ELECTRICAL AND MECHANICAL MODES OF THE hPC

In our description of the nature of the wave propagation modes shown in Figs. 8 and 10, we stated that mode shapes on the mechanical dispersion curves display an—inhomogeneous—electric field distribution in the piezoelectric element as they are dominated by the direct piezoelectric coupling by virtue of which mechanical strain induces a polarization of the actuator. Conversely, mode shapes on the electrical dispersion curves display a homogeneous electric field distribution as the piezoelectric elements are primarily acting as capacitors in the lumped transmission line.

To verify these statements, we studied numerical models of two unit cells without periodic boundary conditions under structural and electrical loading states. The strain fields of the mode shapes at the long and short wavelength limits reveal that the deformations can be approximated by bending moments (higher bending for short wavelengths). Hence, the first unit cell was subjected to bending moments applied at the edges to approximate the deformation of a wave traveling though it (Fig. 11(a)). The second cell was subjected to a potential difference on the piezoelement to simulate the converse piezoelectric effect (Fig. 11(b)). The deformations and electric field distributions are in line with the expectations.

[1]J. J. Hollkamp, "Multimodal passive vibration suppression with piezoelectric materials and resonant shunts," J. Intell. Mater. Syst. Struct. **5**, 49–57 (1994).
[2]B. S. Beck, K. A. Cunefare, M. Ruzzene, and M. Collet, "Experimental analysis of a cantilever beam with a shunted piezoelectric periodic array," J. Intell. Mater. Syst. Struct. **22**, 1177–1187 (2011).
[3]A. Spadoni, M. Ruzzene, and K. Cunefare, "Vibration and wave propagation control of plates with periodic arrays of shunted piezoelectric patches," J. Intell. Mater. Syst. Struct. **20**, 979–990 (2009).
[4]L. Brillouin, *Wave Propagation in Periodic Structures* (McGraw-Hill Book Company, 1946).
[5]P. A. Deymier, *Acoustic Metamaterials and Phononic Crystals* (Springer Science & Business Media, 2013), Vol. 173.
[6]S. Krödel, T. Delpero, A. Bergamini, P. Ermanni, and D. M. Kochmann, "3D auxetic microlattices with independently controllable acoustic band gaps and quasi-static elastic moduli," Adv. Eng. Mater. **15**, 357–363 (2013).
[7]T. T. Wu, Z. G. Huang, T. C. Tsai, and T. C. Wu, "Evidence of complete band gap and resonances in a plate with periodic stubbed surface," Appl. Phys. Lett. **93**, 111902 (2008).
[8]A. Sato, Y. Pennec, T. Yanagishita, H. Masuda, W. Knoll, B. Djafari-Rouhani, and G. Fytas, "Cavity-type hypersonic phononic crystals," New J. Phys. **14**, 113032 (2012).
[9]Z. Liu, "Locally resonant sonic materials," Science **289**, 1734–1736 (2000).
[10]Z. Yang, H. M. Dai, N. H. Chan, G. C. Ma, and P. Sheng, "Acoustic metamaterial panels for sound attenuation in the 50–1000 Hz regime," Appl. Phys. Lett. **96**(4), 041906 (2010).
[11]X. N. Liu, G. K. Hu, G. L. Huang, and C. T. Sun, "An elastic metamaterial with simultaneously negative mass density and bulk modulus," Appl. Phys. Lett. **98**(25), 251907 (2011).
[12]B. R. Mace and E. Manconi, "Wave motion and dispersion phenomena: Veering, locking and strong coupling effects," J. Acoust. Soc. Am. **131**, 1015–1028 (2012).
[13]M. Lapine and S. Tretyakov, "Contemporary notes on metamaterials," Microwaves Antennas Propag. **1**, 3–11 (2007).
[14]J.-H. Lee, J. P. Singer, and E. L. Thomas, "Micro-/nanostructured mechanical metamaterials," Adv. Mater. **24**, 4782–4810 (2012).
[15]J.-F. Robillard, O. Bou Matar, J. O. Vasseur, M. Deymier, A.-C. Stippinger, Y. Pennec, and B. Djafari-Rouhani, "Tunable magnetoelastic phononic crystals," Appl. Phys. Lett. **95**, 124104 (2009).
[16]L. Airoldi and M. Ruzzene, "Wave propagation control in beams through periodic multi-branch shunts," J. Intell. Mater. Syst. Struct. **22**, 1567–1579 (2011).
[17]F. Casadei, T. Delpero, A. Bergamini, P. Ermanni, and M. Ruzzene, "Piezoelectric resonator arrays for tunable acoustic waveguides and metamaterials," J. Appl. Phys. **112**, 064902 (2012).
[18]M. Collet, K. Cunefare, and M. Ichchou, "Wave motion optimization in periodically distributed shunted piezocomposite beam structures," J. Intell. Mater. Syst. Struct. **20**, 787–808 (2008).
[19]A. Bergamini, T. Delpero, L. De Simoni, L. Di Lillo, M. Ruzzene, and P. Ermanni, "Phononic crystal with adaptive connectivity," Adv. Mater. **26**, 1343–1347 (2014).
[20]R. Batra, F. Dell'Isola, S. Vidoli, and D. Vigilante, "Multimode vibration suppression with passive two-terminal distributed network incorporating piezoceramic transducers," Int. J. Solids Struct. **42**, 3115–3132 (2005).
[21]C. Maurini, F. Dell'Isola, and D. Del Vescovo, "Comparison of piezoelectronic networks acting as distributed vibration absorbers," Mech. Syst. Signal Process. **18**, 1243–1271 (2004).
[22]F. Dell'Isola, C. Maurini, and M. Porfiri, "Passive damping of beam vibrations through distributed electric networks and piezoelectric transducers: prototype design and experimental validation," Smart Mater. Struct. **13**, 299–308 (2004).
[23]M. Reddy, "Some new operational-amplifier circuits for the realization of the lossless floating inductance," IEEE Trans. Circuits Syst. **23**(3), 171–173 (1976).
[24]M. Remoissenet, *Waves Called Solitons: Concepts and Experiments* (Springer Science & Business Media, 1999).
[25]T. J. Cui, D. R. Smith, and R. Liu, *Metamaterials* (Springer, 2010).
[26]F. Casadei, M. Ruzzene, L. Dozio, and K. A. Cunefare, "Broadband vibration control through periodic arrays of resonant shunts: Experimental investigation on plates," Smart Mater. Struct. **19**, 015002 (2010).

[27]J. Sólyom, *Fundamentals of the Physics of Solids: Volume 3-Normal, Broken-Symmetry, and Correlated Systems* (Springer Science & Business Media, 2010), Vol. 3.
[28]T. Gorishnyy, J.-H. Jang, C. Y. Koh, and E. L. Thomas, "Direct observation of a hypersonic band gap in two-dimensional single crystalline phononic structures," Appl. Phys. Lett. **91**, 121915 (2007).
[29]L. Airoldi and M. Ruzzene, "Design of tunable acoustic metamaterials through periodic arrays of resonant shunted piezos," New J. Phys. **13**(11), 113010 (2011).
[30]L. Cremer and M. Heckl, *Structure-Borne Sound: Structural Vibrations and Sound Radiation at Audio Frequencies* (Springer Science & Business Media, 2013).